



HAL
open science

EMI Study of Three-Phase Inverter-Fed Motor Drives

Bertrand Revol, James Roudet, Jean-Luc Schanen, Philippe Loizelet

► **To cite this version:**

Bertrand Revol, James Roudet, Jean-Luc Schanen, Philippe Loizelet. EMI Study of Three-Phase Inverter-Fed Motor Drives. IEEE Transactions on Industry Applications, 2011, 47 (1), pp.223-231. 10.1109/TIA.2010.2091193 . hal-00578202

HAL Id: hal-00578202

<https://hal.science/hal-00578202>

Submitted on 18 Mar 2011

HAL is a multi-disciplinary open access archive for the deposit and dissemination of scientific research documents, whether they are published or not. The documents may come from teaching and research institutions in France or abroad, or from public or private research centers.

L'archive ouverte pluridisciplinaire **HAL**, est destinée au dépôt et à la diffusion de documents scientifiques de niveau recherche, publiés ou non, émanant des établissements d'enseignement et de recherche français ou étrangers, des laboratoires publics ou privés.

EMI Study of Three-Phase Inverter-Fed Motor Drives

Bertrand Revol, James Roudet, Jean-Luc Schanen, *Senior Member, IEEE*, and Philippe Loizelet

Abstract—Today, electromagnetic compatibility (EMC) seems to be one of the major constraints of power electronic converters, particularly for variable-speed drives. Unfortunately, it is too often regarded as the last phase of the development of a converter since it represents the last step of its marketing. The estimation of conducted and radiated disturbances by simulation offers a considerable gain from the economic point of view. This paper shows how relatively simple models can be used to forecast EMC, taking into account various control strategies. These models are validated on an experimental setup and can be used during the design of a variable-speed inverter motor association. The objective is to approach by “fast” simulations the conducted emission to consider optimization processes. It is then imperative to take into account the environment of the converter, which implies the modeling of cables, motors, and, naturally, the filters.

Index Terms—Electromagnetic compatibility (EMC), modeling, simulation, variable-speed drives.

I. INTRODUCTION

THE DESIGN of a variable-speed drive must not only take into account external performance, such as speed and torque, but also of more technological parameters, such as efficiency and electromagnetic compatibility (EMC) aspects.

Designing a system with only one of these objectives will necessary lead to a nonoptimal result and sometimes to a “redesign” task, which is costly and time consuming.

The aim of this paper is to propose relatively simple models of all phenomena involved in an inverter–motor association in order to depict the influence of elements, such as the electromagnetic interference (EMI) filter, the ac motor, and the feeder. The requirements of this model are to give the right tendencies with quick computation times, rather than to be the most precise. Temporal simulations are too long to meet these requirements, and alternative solutions must be proposed. With the proposed model, various control strategies can be

Manuscript received October 31, 2004; accepted June 23, 2010. Date of publication November 9, 2010; date of current version January 19, 2011. Paper IPCSD-2010-001, presented at the 2004 Industry Applications Society Annual Meeting, Seattle, WA, October 3–7, and approved for publication in the IEEE TRANSACTIONS ON INDUSTRY APPLICATIONS by the Power Electronics Devices and Components Committee of the IEEE Industry Applications Society. This work was supported by Schneider Toshiba Inverter Europe (STIE).

B. Revol is with the Systemes et Applications des Technologies de l'Information et de l'Energie (SATIE), ESN Cachan, 94235 Cachan Cedex, France.

J. Roudet and J.-L. Schanen are with the Grenoble Electrical Engineering Laboratory (G2ELab), CNRS UMR 5269 UJF/INP, Domaine Universitaire, 38402 Saint Martin d'Hères Cedex, France (e-mail: jean-luc.schanen@g2elab.grenoble-inp.fr).

P. Loizelet is with Schneider Toshiba Inverter Europe, 27120 Pacy sur Eure, France.

Color versions of one or more of the figures in this paper are available online at <http://ieeexplore.ieee.org>.

Digital Object Identifier 10.1109/TIA.2010.2091193

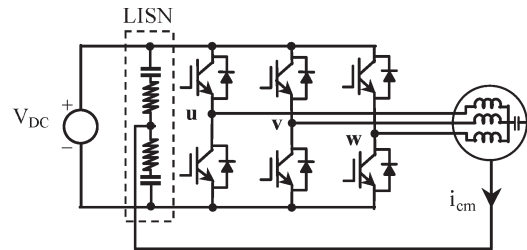


Fig. 1. Simplified schema of the inverter.

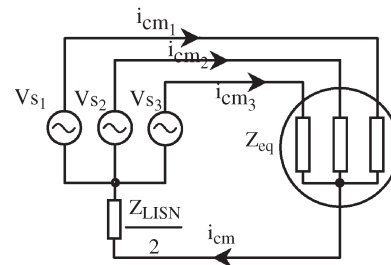


Fig. 2. Common-mode equivalent schema.

investigated: simple sine-wave pulsewidth modulation (PWM), with or without third harmonic, triplen, dead-banded triplen, and space-vector modulation. The technical realization can be also taken into account (triangular or sawtooth carrier signals).

Section II will describe the different EMC models. Experimental verification will confirm the pretty accuracy of these models. The last part introduces a sensitive study carried out by the effect of cable length on the common-mode capacitance.

II. EMC MODELS

A. Model of the Inverter

The EMC modeling of the three-phase inverters has, as a common objective, the reduction of the disturbances generated by this type of equipment [1]. This paper is based on the transformation of a variable topology (static converter Fig. 1) to a linear electrical circuit where all passive components and most important parasitic elements and propagation paths are defined [2], [3]. An analysis of the sources and spreading paths of the interference signals is necessary to quantify the EMI. The main sources of conducted and radiated electromagnetic perturbations are the active elements.

1) *Classical Study of the Common Mode*: Basically, the different studies already published focus on the common-mode disturbances. Generally, this mode is considered as the most disturbing one on the conducted frequency range and constitutes the most difficult to cancel. With this assumption, many models can be carried out, like the following, which are basically the simplest for such structures (Fig. 2). Three voltage

sources are required for these models to point out the dV/dt effects of the three switching cells. The main propagation paths are defined owing to the equivalent impedance of the load (motor and feeder) per phase Z_{eq} and the line impedance stabilization network (LISN) impedance Z_{LISN} . This simple model is based on the symmetry of the propagation paths that explains the half impedance of the LISN that is supposed to be in parallel.

The common-mode current is given by the very simple expression (1). The main interest of this relation is to highlight the equivalent common-mode source V_{CM} which corresponds to the sum of the three initial sources (2). This particular source is a multilevel tension whose amplitude lies between $-V_{DC}/2$ and $V_{DC}/2$, whatever the PWM control is

$$i_{cm} = \frac{1}{\frac{Z_{eq}}{3} + \frac{Z_{LISN}}{2}} \cdot V_{CM} \quad (1)$$

$$V_{CM} = \frac{V_{S1} + V_{S2} + V_{S3}}{3}. \quad (2)$$

Unfortunately, this model is too restrictive to explain all the EMI phenomena in the inverter. For example, the common-mode current due to asymmetrical propagation paths cannot be highlighted. This current appears when stray capacitances or the filter's capacitors placed between the copper power circuit layer and the ground are not exactly equal.

2) *Differential Mode*: The differential-mode mechanisms are quite simple to present (Fig. 3). Although this mode is dominant for low frequencies around the switching frequency,

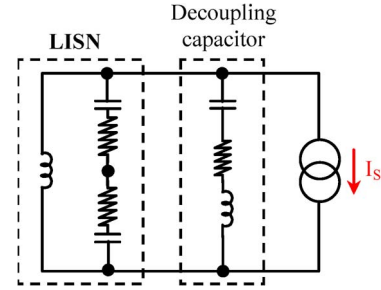


Fig. 3. Differential mode equivalent schema.

it must be taken into account. As a matter of fact, without a correct estimation of the entrance current linked to this mode, the elements of the EMI filters cannot be sized correctly. Thus, it can be carried out by an equivalent current source which is defined with the three switched currents of the inverter cells detailed in the following paragraphs. The decoupling equivalent capacitor represents the first filtering element to limit the current's harmonics in the power supply. The disturbance's spectrum due to the differential mode depends on the quality of capacitors used on the dc bus.

3) *Global Representation of the Inverter*: The strong current and voltage variations from the switching cell permit the creation of a linear simplified equivalent simulation circuit (Fig. 4). The transfer functions generally used in the EMI studies are too complex to express with such structures. They are also source of errors. To avoid this calculation method, a matrix form is used, as shown in (3), at the bottom of the page. The elements are determined with a simple graphical technique based on a

$$\begin{pmatrix} I_1 \\ I_2 \\ I_3 \\ I_4 \\ I_5 \\ I_6 \\ I_7 \\ I_8 \\ I_9 \\ I_{10} \\ I_{11} \\ V_{I_s} \end{pmatrix} = \begin{pmatrix} Z_{me1} & -Z_t & -Z_t & Z_t & 0 & 0 & 0 & 0 & 0 & 0 & 0 & 0 & 0 \\ * & Z_{me2} & Z_t & -Z_t & 0 & 0 & 0 & 0 & 0 & 0 & 0 & 0 & 0 \\ * & * & Z_{me3} & Z_{CMC} & -Z_{cp} & -Z_{cp} & -Z_{cp} & -Z_{cp} & 0 & 0 & 0 & 0 & 0 \\ * & * & * & Z_{me4} & Z_{cm} & Z_{cm} & Z_{cm} & Z_{cm} & -Z_{cm} & -Z_{cm} & -Z_{cm} & 0 & 0 \\ * & * & * & * & Z_{me5} & Z_{cf} & Z_{cf} & Z_{cf} & Z_{cm} & Z_{cm} & Z_{cm} & 0 & 0 \\ * & * & * & * & * & Z_{me6} & Z_{bf} & Z_{bf} & -Z_{bfm} & -Z_{bfm} & -Z_{bfm} & 0 & 0 \\ * & * & * & * & * & * & Z_{me7} & Z_{bf} & -Z_{bfm} & -Z_{bfm} & -Z_{bfm} & 0 & 0 \\ * & * & * & * & * & * & * & Z_{me8} & -Z_{bfm} & -Z_{bfm} & -Z_{bfm} & 0 & 0 \\ * & * & * & * & * & * & * & * & Z_{me9} & Z_{bfm} & Z_{bfm} & 0 & 0 \\ * & * & * & * & * & * & * & * & * & Z_{me10} & Z_{bfm} & 0 & 0 \\ * & * & * & * & * & * & * & * & * & * & Z_{me11} & 0 & 0 \\ 0 & 0 & -Z_{cp} & Z_{cm} & Z_{cf} & Z_{bf} & Z_{bf} & Z_{bf} & Z_{bf} & -Z_{bfm} & -Z_{bfm} & -Z_{bfm} & 1 \end{pmatrix}^{-1} \begin{pmatrix} 0 \\ 0 \\ Z_{cp} \cdot I_s \\ -Z_{cm} \cdot I_s \\ -Z_{cf} \cdot I_s \\ -V_{S1} - Z_{bf} \cdot I_s \\ -V_{S2} - Z_{bf} \cdot I_s \\ -V_{S2} - Z_{bf} \cdot I_s \\ Z_{bfm} \cdot I_s \\ Z_{bfm} \cdot I_s \\ Z_{bfm} \cdot I_s \\ -Z_{bf} \cdot I_s \end{pmatrix} \quad (3)$$

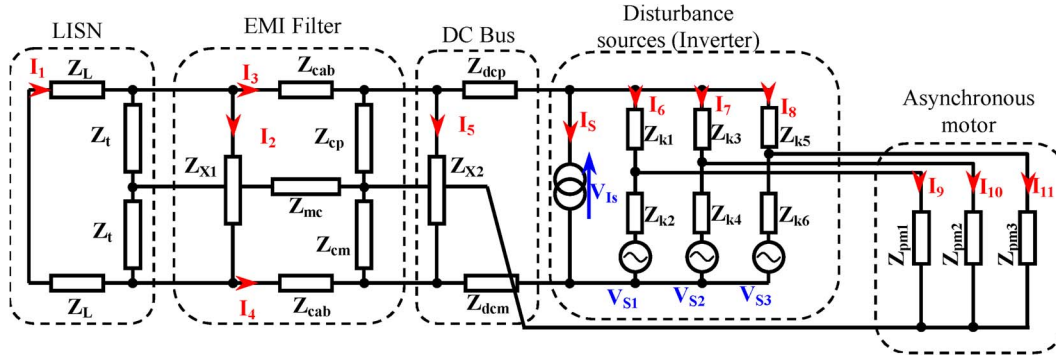


Fig. 4. Linear equivalent circuit of the variable-speed drive system.

particular choice of currents in each electric mesh for which Kirchoff's laws are very simple to define. With this method, both types of sources are treated simultaneously.

The voltage and current disturbance sources are defined with analytical expressions. They are directly defined in the frequency domain for each harmonic n of the modulating frequency owing to Laplace transforms, knowing the switching times (t_{on}, t_{off}) of phase p from the PWM strategy used. The switching times are given owing to an algorithm based on a Newton method. The derivative signals are required in such algorithms. With these useful signals, a very low number of iterations are required for great precision. Owing to this calculation method, all PWM types can be treated. If the voltage is relatively simple to express with a sum of elementary trapezoidal signals (4), the current source is more difficult to obtain. It is defined, knowing the current's magnitude I_M and the phase shift ϕ between the voltage and current in each phase of the motor. Naturally, this current depends on the three switching functions defined by the PWM strategy. The elementary trapezoidal signal ($Trap_{i,p}$) of the i th switching period depending on phase p is given by (5). Thus, the analytical expression of the rectified current (6), presented in this paper, is also generic and can be used, whatever the PWM control is [see (3), shown at the bottom of the previous page]. Here,

$$Z_{me1} = 2(Z_L + Z_t)$$

$$Z_{me2} = 2Z_t + Z_{X1}$$

$$Z_{me3} = Z_{cab} + Z_t + Z_{cp} + Z_{CMC}$$

$$Z_{me4} = Z_{cab} + Z_t + Z_{cm} + Z_{CMC}$$

$$Z_{me5} = Z_{X2} + Z_{cp} + Z_{cm}$$

$$Z_{me6} = Z_{k1} + Z_{k2} + Z_{bf}$$

$$Z_{me7} = Z_{k3} + Z_{k4} + Z_{bf}$$

$$Z_{me8} = Z_{k5} + Z_{k6} + Z_{bf}$$

$$Z_{me9} = Z_{k2} + Z_{bfm} + Z_{mp1}$$

$$Z_{me10} = Z_{k4} + Z_{bfm} + Z_{mp2}$$

$$Z_{me11} = Z_{k6} + Z_{bfm} + Z_{mp3}$$

$$Z_{bf} = Z_{cf} + Z_{dcp} + Z_{dcm}$$

$$Z_{cf} = Z_{cp} + Z_{cm}$$

$$Z_{bfm} = Z_{cm} + Z_{dcm}$$

$$(V_{S_p})_n = V_{dc} \cdot \sum_{i=0}^{N-1} \frac{1}{2 \cdot \pi \cdot j \cdot n} \cdot \left(\text{sinc}\left(\frac{t_m \cdot n}{T_S}\right) \cdot e^{-\pi \cdot j \cdot n \cdot \frac{2 \cdot t_{off_{i,p}} + t_m}{T_S}} - \text{sinc}\left(\frac{t_d \cdot n}{T_S}\right) \cdot e^{-\pi \cdot j \cdot n \cdot \frac{2 \cdot t_{on_{i,p}} + t_d}{T_S}} \right) \quad (4)$$

with $\text{sinc}(x) = \sin(x)/x$

V_{DC} dc voltage source;

t_m rise time;

t_{on}, t_{off} switching times;

t_d fall time;

N number of switching periods;

T_S electrical frequency of the motor (defined by PWM);

and see (5) and (6), at the bottom of the page.

Although the complexity of the switching-transition waveforms is not exactly represented, good frequency behavior can be expected depending on the desired limit frequency. Furthermore, inverse fast Fourier transforms can be used to pass easily between both domains choosing $n = 0, \dots, 2^P$ (P is an integer) once the signals are defined in the frequency domain.

$$Trap_{i,p}(v) = \frac{1}{T_S} \cdot \frac{\text{sinc}(t_m \cdot v) \cdot e^{-\pi \cdot j \cdot (2 \cdot t_{on_{i,p}} + t_m) \cdot v} - \text{sinc}(t_d \cdot v) \cdot e^{-\pi \cdot j \cdot (2 \cdot t_{off_{i,p}} + t_d) \cdot v}}{2 \cdot \pi \cdot j \cdot v} \quad (5)$$

$$I_{S_n} = \frac{I_M}{2 \cdot j} \cdot \sum_{p=0}^2 \sum_{i=0}^{N-1} \left[Trap_{i,p} \left(\frac{n-1}{T_S} \right) \cdot e^{-j \cdot (p \frac{2\pi}{3} - \phi)} - Trap_{i,p} \left(\frac{n+1}{T_S} \right) \cdot e^{-j \cdot (p \frac{2\pi}{3} - \phi)} \right] \quad (6)$$

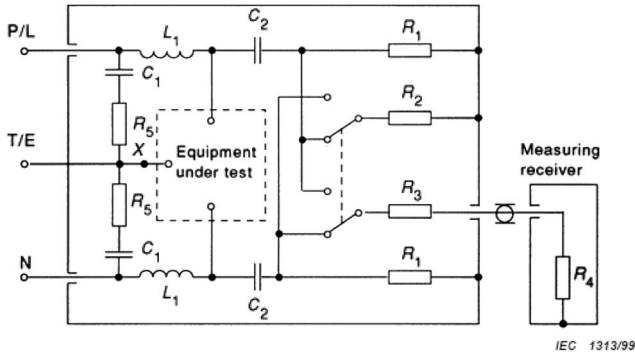


Fig. 5. Measurement protocol of the impedances used for identification.

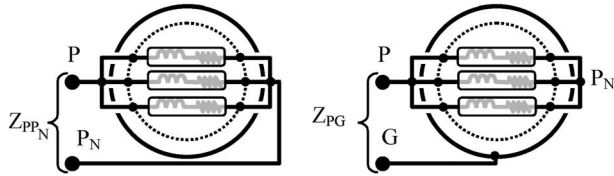


Fig. 6. Measurement protocol of the impedances used for identification.

B. Discussion About the LISN

LISN is defined according to International Special Committee on Radio Interference 16 standards [4] and shown in Fig. 5. The dynamic imposed by the different elements of such structure penalizes the time-domain simulation transient in addition to very small calculation step. In this frequency approach, the LISN is replaced with impedance constituting the main components and their stray elements. In Fig. 4, Z_L corresponds to the line inductance of the LISN, and Z_t corresponds to the normalized measurement impedance. Basically, the perfect dc source is not represented on the frequency equivalent circuit; however, average values are taken into account in the source description, as presented earlier. Thus, the first stage of the scheme represented by the LISN allows EMI computation. The estimated spectrum is deduced from the LISN 50-Ω impedances. The real LISN particularly developed and used for this paper gives correct measurements from 10 to 20 MHz. This frequency-range limit is sufficient to present the main EMI phenomena in this case.

C. Motor Modeling

One of the main propagation paths is constituted by the ac motor and the feeder. The presented model, based on classical high-frequency models [3], is mainly defined for common-mode current. Nevertheless, this approach allows defining the impedances of the motor windings. Thus, the current in all phases can be estimated to determine the current disturbance source placed on the dc bus. The parameter identification consist in the measurement of two impedances Z_{PPN} and Z_{PG} (Fig. 6). The first one is measured between the free phase terminals connected together with the floating ground terminal. The second one is measured between the short-circuited windings and the ground terminal defined by the frame of the motor. Both are extracted from an impedance analyzer HP4194A, which

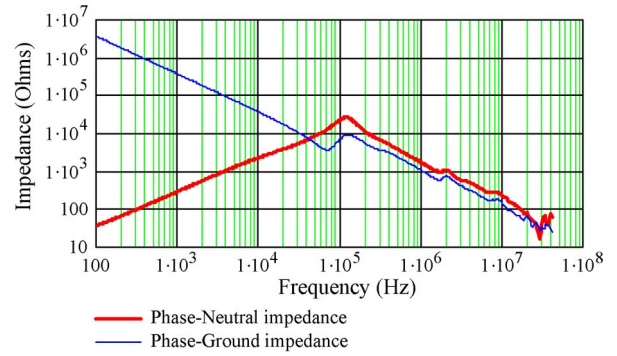


Fig. 7. Main impedances of the ac motor used (AEG750W).

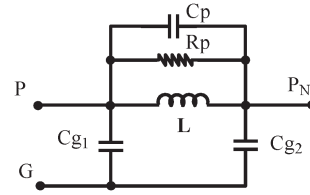


Fig. 8. Simplified high-frequency model for one phase.

allows a frequency range between 100 Hz and 40 MHz (Fig. 7). The equivalent schemes typically used are generally based on the physical representation phenomena. For example, the following one (Fig. 8) represents the main elements of a motor winding [5], [6]. The parasitic capacitor of one winding is given by C_p . The winding to the ground-distributed capacitance has been represented by two lumped capacitances: C_{g1} and C_{g2} . The first one is connected between the phase terminal (P) and the ground (G), and the second one is connected between the motor neutral (P_N) and the ground (G). In the first part of the frequency range, the serial resistor of each winding can be neglected compared with the reactance of the inductance L . With such equivalent schema, the simple impedance expressions (7) and (8) are obtained for both configurations, and a simple study based on particular measured frequencies can be highlighted. Moreover, both impedances have a common denominator that corresponds to a common resonance frequency. The experimental results presented previously confirm this principle

$$Z_{PPN} = \frac{1}{3} \cdot \frac{L \cdot p}{L \left(C_P + \frac{C_{g1}C_{g2}}{C_{g1}+C_{g2}} \right) p^2 + \frac{L}{R_P} p + 1} \tag{7}$$

$$Z_{PG} = \frac{L(C_P + C_{g2})p^2 + \frac{L}{R_P}p + 1}{6C_{g1}p \left(L \left(C_P + \frac{C_{g1}C_{g2}}{C_{g1}+C_{g2}} \right) p^2 + \frac{L}{R_P}p + 1 \right)} \tag{8}$$

Two characteristic frequencies are extracted from the phase-ground impedance (Fig. 9). The first one $F_{N(PG)}$ represents the natural frequency of the Z_{PG} numerator (9) that minimizes the impedance. A similar frequency $F_{D(PG)}$ is obtained from the denominator and defines the impedance resonance

$$F_{N(PG)} = \frac{1}{2\pi\sqrt{L \cdot (C_P + C'_{g2})}} \tag{9}$$

$$F_{D(PG)} = \frac{1}{2\pi\sqrt{L \cdot (C_P + k \cdot C_{g2})}} \tag{10}$$

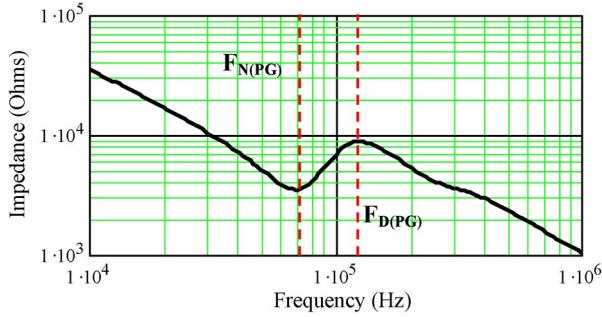


Fig. 9. Resonances of the common-mode impedance.

with

$$k = \frac{\alpha}{1 + \alpha}, \quad \alpha = \frac{C_{g1}}{C_{g2}}.$$

Defining the ratio r of $F_{D(PG)}$ to $F_{N(PG)}$, a relationship between C_P and C_{g2} is obtained

$$\beta = \frac{1 - k \cdot r^2}{r^2 - 1} \quad \text{with} \quad \beta = \frac{C_P}{C_{g2}}, \quad r = \frac{F_{D(PG)}}{F_{N(PG)}}. \quad (11)$$

This last expression allows defining β (i.e., C_P) with the parameter k . Thus, the sign of β depends on the choice of k . According to the hypothesis that C_{g2} is a positive element, the following cases about k can be used to determine C_P .

Case 1: $k = 1/r^2$ leads to $C_P = 0$.

Case 2: $k > 1/r^2$ leads to $C_P < 0$.

Case 3: $k < 1/r^2$ leads to $C_P > 0$.

Furthermore, to obtain positive values of C_{g1} , k must be selected between zero and one.

The sum of the capacitances C_{g1} and C_{g2} are evaluated assuming that the measured phase-ground impedance is purely capacitive for low frequency (under 1 kHz), and the reactance is negligible. Knowing the measured phase-ground impedance modulus $Z_{m_{PG}}$ at the lowest frequency F_{LF} , the capacitance C_{g2} is given by

$$C_{g2} = \frac{1 - k}{Z_{m_{PG}} \cdot 2\pi \cdot F_{LF}}. \quad (12)$$

A particular discussion is required about the value of the inductance L . The equivalent inductance when the three motor phases are short circuited corresponds to a linear combination of the self- and the mutual inductance (L_P and M_P) of the stator (13). Indeed, this inductance, measured with the phase-neutral impedance, is restricted to the common-mode current. It cannot be used to evaluate the real-power current directly

$$L = L_P + 2 \cdot M_P. \quad (13)$$

However, special attention is paid to this inductance seen by the common-mode current. L is modeled by an electrical equivalent schema in staircase (Fig. 10). Such models are generally used to take into account eddy currents and proximity effects in transformer windings and can be also used for motors (Fig. 11). The parameters of such models are generally difficult to evaluate. However, for a relatively low number of elements,

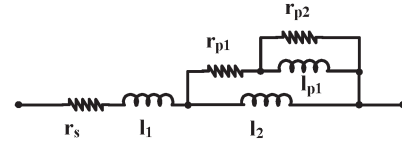
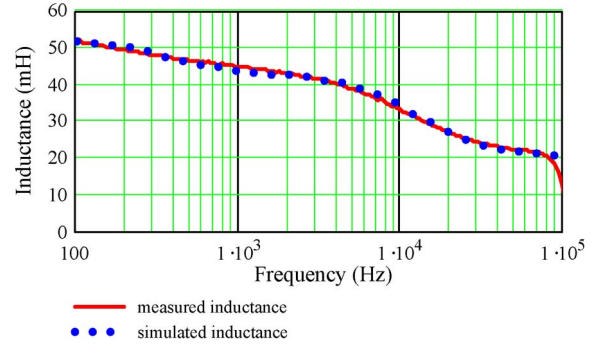

 Fig. 10. Electrical equivalent schema in staircase of a winding (AEG750W). ($r_s = 5 \Omega$, $r_{p1} = 221 \Omega$, $r_{p2} = 1554 \Omega$, $l_1 = 20 \text{ mH}$, $l_2 = 32 \text{ mH}$, and $l_{p1} = 60 \text{ mH}$).

Fig. 11. Evolution of the inductance seen by the common-mode current.

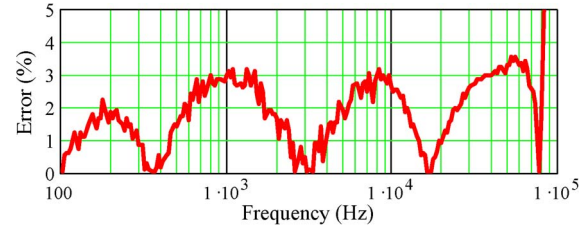
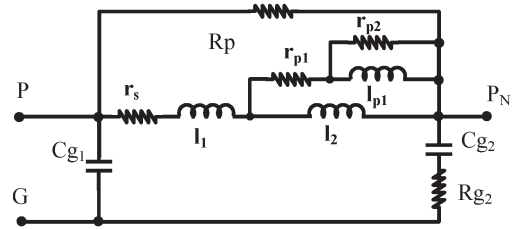


Fig. 12. Relative error between the model and the measurement.


 Fig. 13. Electrical equivalent schema of the motor winding (AEG750W) ($R_p = 30 \text{ k}\Omega$, $C_{g1} = 138 \text{ pF}$, $C_{g2} = 332 \text{ pF}$, and $R_{g2} = 1 \text{ k}\Omega$).

resolution algorithms of nonlinear systems can be used. In our case, this technique gives good results. Indeed, the relative error between the measured inductance and that of the model remains lower than 4% for frequencies before the resonance due to capacitive effects (Fig. 12).

For the tested motor, the solution with $C_p = 0$ is chosen to point out the fickleness of this behavioral model. Two other parameters are added to define damping effects. The iron losses can be represented by the resistor R_P , defined with the maximum value of the phase-neutral impedance. R_{g2} allows limiting serial resonance of the impedance (Fig. 13). The good agreements between simulations and measurements are presented hereafter (Figs. 14 and 15).

In this study, a motor star connection has been assumed. Furthermore, this model is not changed with a delta connection,

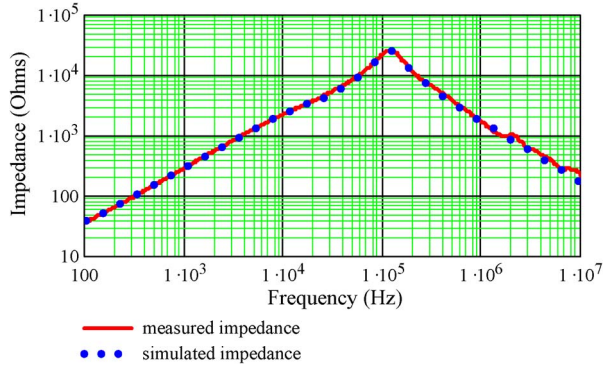


Fig. 14. Comparison between measurement and the model for the phase-neutral impedance.

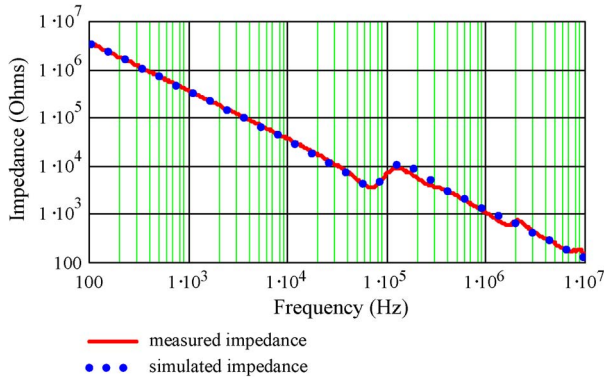


Fig. 15. Measurement and the model for the phase-ground impedance.

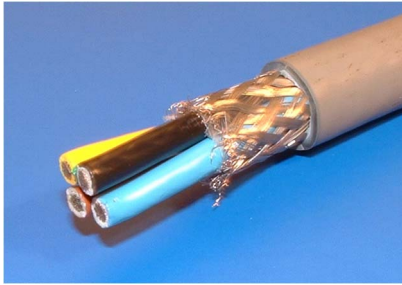


Fig. 16. Shielded three-phase cable studied.

and usual transformations make it possible to pass from one to the other.

D. Cable Modeling

The considered cable in this study, between the inverter and the motor, is a shielded three-phase cable, including a fourth conductor bound to earth. This conductor ensures human and equipment protection. It is shown in Fig. 16. Since the cable length is often several meters, propagation effects cannot be neglected. During the outdoor emission tests for long cables (5–10 m), the shield becomes necessary to respect EMC standards limiting radiated emissions. Moreover, the presence of a shield permits an easy use of high-frequency methods for parameter extraction since a “natural” ground exists: the shielding conductor. More directly, the per-unit length parameters can

TABLE I
CABLE PARAMETERS OBTAINED WITH HP4194A, FOR
LOW (5-kHz) AND HIGH (40-MHz) FREQUENCIES

Parameters	Frequency	
	5 kHz	30 MHz
L (nH/m)	328	197
C (pF/m)	295	262

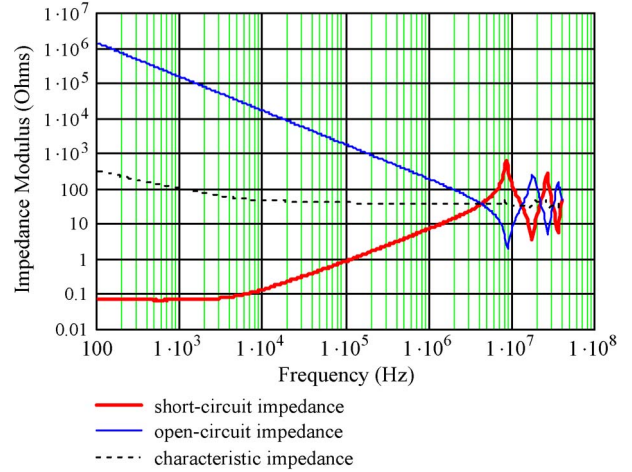


Fig. 17. Impedance measurements of the shielded cable (5 m).

be obtained by measuring the short-circuited cable for L and open-circuited cable for C and dividing by the cable length (Table I). We can notice that the frequency effect on both elements (L and C) is clearly shown with these measurements.

To simulate the influence of the length D of a long cable taking into account the propagation phenomena, a propagation matrix Φ (14) can be expressed. These effects can be noticed on the impedance curves owing to the resonance phenomena for high frequencies (Fig. 17). This matrix makes it possible to express the electric quantities at the exit of the cable according to those of the entrance. To define the different submatrix ϕ_{ij} (15), the eigenvalues γ and their associated matrix T are required (16). The matrix impedance and admittance (Z, Y) are given either by measurement or by analytical formulas [7]. The total impedance (Z_0) of the cable and the motor as seen by the inverter is defined in (17). The terminal impedance matrix Z_L is defined by the equivalent electrical scheme of the motor

$$\begin{pmatrix} V_L \\ I_L \end{pmatrix} = \begin{pmatrix} \Phi_{11} & \Phi_{12} \\ \Phi_{21} & \Phi_{22} \end{pmatrix} \cdot \begin{pmatrix} V_0 \\ I_0 \end{pmatrix} \quad (14)$$

$$\Phi_{11} = Y^{-1} T \cdot \text{ch}(\gamma \cdot D) \cdot T^{-1} Y$$

$$\Phi_{12} = Z_C \cdot T \cdot \text{sh}(\gamma \cdot D) \cdot T^{-1}$$

$$\Phi_{21} = -T \text{sh}(\gamma \cdot D) \cdot T^{-1} Y_C$$

$$\Phi_{22} = T \cdot \text{ch}(\gamma \cdot D) \cdot T^{-1} \quad (15)$$

with $Z_C = Z \cdot T \cdot \gamma \cdot T^{-1}$, and $Y_C = Z_C^{-1}$

$$\gamma^2 = T^{-1} Y \cdot Z \cdot T \quad (16)$$

$$Z_0 = (Z_L \cdot \Phi_{21} - \Phi_{11})^{-1} \cdot (\Phi_{12} - Z_L \cdot \Phi_{22}). \quad (17)$$

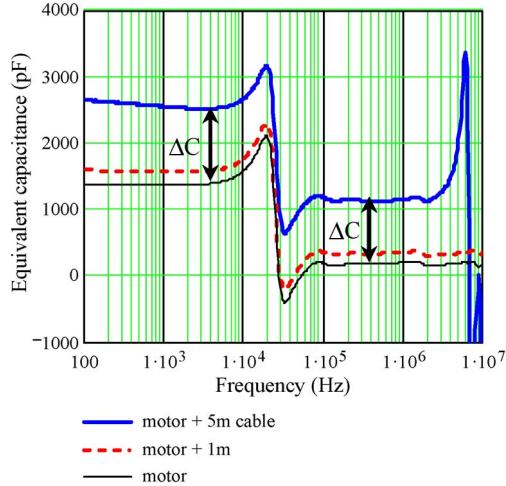


Fig. 18. Evolution of the phase-ground equivalent capacitance with cable length.

The feeder, the induction motor, and the stray capacitances of the power module are gathered to define the load impedance Z_{pm} , previously mentioned in the EMC matrix of the global model.

III. SENSITIVITY STUDY AND RESULTS

A. Total Stray Capacitance

Taking into account the values of capacitance phase-ground and neutral-ground capacitors, the motor constitute one of the most important propagation path of common-mode current. The measurements shown in Fig. 18 show the decrease of phase-ground impedance due to the increase of the capacitance when the cable length increases. The equivalent capacitor of the phase-ground impedance is shown in the next figure (Fig. 13). If only the motor is considered, the equivalent capacitor on the conducted frequency bandwidth (150 kHz–30 MHz) is about 200 pF.

This value, which increases, reaching 1 nF for cable length of 5 m, had to be compared with the parasitic capacitors of the power module (20–200 pF) [8]. Thus, the cable and the motor impedance have to be taken into account for correct estimation of the common-mode currents circulating along this path. The disturbance spectrum level on the LISN increases considerably with cable length.

B. Importance of the Spectrum Analyzer

A superheterodyne spectrum analyzer (HP8560A) has been used in this study. The video filter is one of the most important stages of such equipments for its functioning and for EMC measurements. This filter defines the radio bandwidth (RBW) imposed by standards and used for the detection of disturbance level. If the RBW is larger than the frequency difference of two lines in the spectrum, they are gathered (Fig. 19). Depending on the equipment under test, the EMC-standard-defined special RBW of 0.9 kHz is generally used for power converters (CISPR 16 [4]). Thus, if the lines of the spectrum are in a distant of

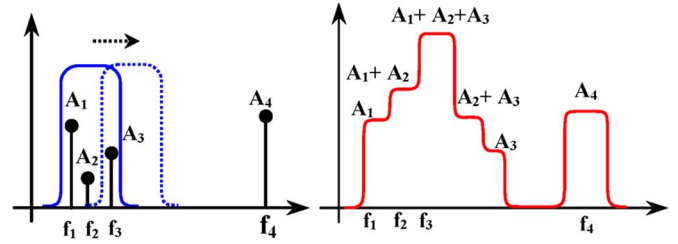


Fig. 19. Modification of the spectrum due to the analyzer.

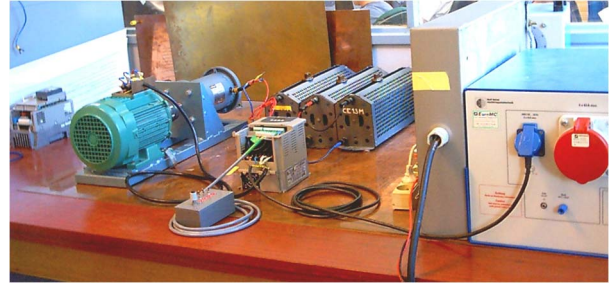


Fig. 20. Experimental setup.

more than 9 kHz, the analyzer has few effects on the spectrum. On the contrary case, it must be taken into account. The theoretical response of the filter used has been modeled with a frequency function (18). Thus, the effects of this filter are applied, convoluting the estimated spectrum of the disturbances S with the function of the filter F (19)

$$F_{\nu_0}(\nu) = \left[\frac{1}{\sqrt{1 + \lambda \cdot (\nu - \nu_0)^2}} \right]^N \quad (18)$$

with

$$\lambda = \frac{4}{RBW^2} \cdot \left(e^{\frac{3 \cdot \ln(10)}{10N}} - 1 \right) \quad (19)$$

$$S_F(\nu) = S(\nu) \otimes F_{\nu_0}(\nu).$$

C. Experimental Setup

The experimental setup, shown in the following figure (Fig. 20), is made up of an industrial LISN, a commercial PWM inverter of 1.5 kW (Altivar 28 Télémécanique), and an asynchronous motor (AEG 750 W). The load of the ac motor is constituted by a dc generator connected to a system of resistors. All equipment lies on a copper plate connected to the ground. These types of inverter are generally used in small industrial applications, such as conveyor chains or ventilation units.

D. Results

To evaluate, the analytical approach is compared with the measurement on the experimental setup previously detailed. For these results, the dc generator is not connected to the resistors. This case is proposed to privilege common-mode disturbances. Moreover, the EMI filter has been disconnected to point out the high level of the disturbances. The PWM used in this inverter has been correctly identified to define the four

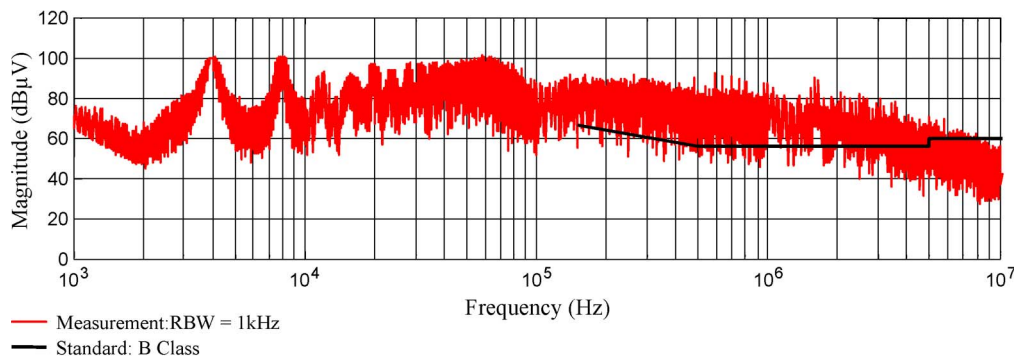


Fig. 21. Measurement of the conducted EMI on the LISN.

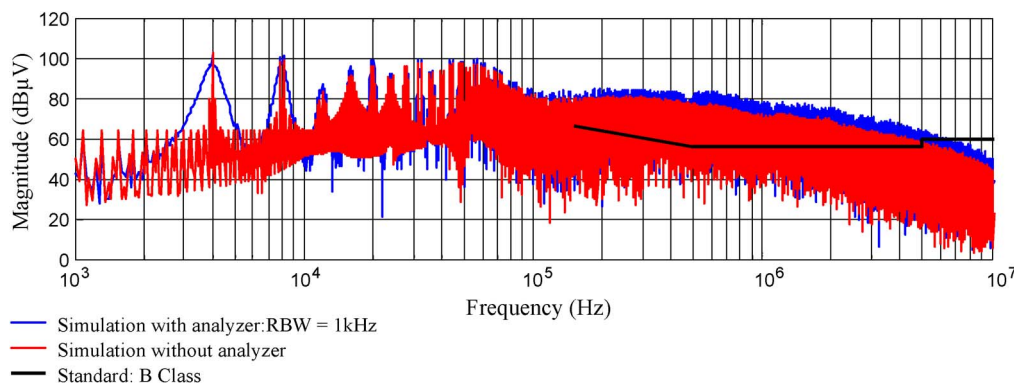


Fig. 22. Simulation of the conducted EMI on the LISN.

disturbance sources of the model. The switching frequency is fixed at 4 kHz. The good agreement between the experimental and the simulation results obtained by the proposed model is well evident (Figs. 21 and 22).

IV. CONCLUSION

The prediction method proposed has permitted fast and robust simulations, taking into account all passive components. This method consists in replacing the switching cells of an inverter by current and voltage sources, defined in the frequency domain. This permits highlighting the negative effects of the stray elements of the structure and the importance of the motor and cable propagation paths. The results of the model agree with the experimental tests in the radio bandwidth (150 kHz–30 MHz). The simulation times have been considerably reduced owing to this frequency approach. The SABER simulation time is up to 15 min against 15 s for the MATLAB simulation. This work has made it possible to carry out the total optimization of the variable-speed drives taking into account the EMC constraints. This study will permit converter builders to reduce the number of prototypes and to include the EMC study in the engineering development of the product.

REFERENCES

- [1] G. Grandi and D. Casadei, "Analysis of common and differential mode HF current components in PWM inverter-fed AC motors," in *Proc. IEEE PESC*, Fukuoka, Japan, 1998, pp. 1146–1151.
- [2] A. Consoli and G. Oriti, "Induction motor modeling for common mode and differential mode emission evaluation," in *Conf. Rec. IEEE IAS Annu. Meeting*, San Diego, CA, Oct. 7–11, 1996, pp. 595–599.

- [3] A. Boglietti and E. Carpaneto, "Induction motor high frequency model," in *Conf. Rec. 34th IEEE IAS Annu. Meeting*, 1999, vol. 3, pp. 1551–1558.
- [4] *Specification for Radio Disturbance and Immunity Measuring Apparatus and Methods*, CISPR 16 Standard. CISPR 16-1 CEI:1996+A1:1999.
- [5] B. Revol, J.-L. Schanen, J. Roudet, and Y. Souhard, "EMI modeling of an inverter—Motor association," in *Proc. CPE*, Gdansk, Poland, 2003, pp. 86–95.
- [6] B. Revol, J. Roudet, and J. L. Schanen, "Fast EMI prediction method for three-phase inverter based on Laplace transforms," in *Conf. Rec. IEEE PESC*, Acapulco, Mexico, 2003, pp. 1133–1138.
- [7] C. R. Paul, *Analysis of Multiconductor Transmission Lines*. Hoboken, NJ: Wiley, 1992.
- [8] C. S. Walker, *Capacitance, Inductance and Crosstalk Analysis*. Norwood, MA: Artech House, 1990.



Bertrand Revol was born in France in 1976. He received the Diploma in electrical engineering from the Grenoble Institute of Technology, Grenoble, France, in 2000 and the Ph.D. degree in electrical engineering from the University Joseph Fourier, Grenoble, in 2003.

He is currently with the Systemes et Applications des Technologies de l'Information et de l'Energie (SATIE), ENS Cachan, Cachan, France, where he carries out research works on the improvement of the electromagnetic-interference filtering optimization.

His principal fields of research relate to the electromagnetic compatibility of power-electronic converters.



James Roudet was born in 1963. He received the Engineer and Ph.D. degrees in electrical engineering from the Institut Polytechnique de Grenoble, Grenoble, France, in 1986 and 1990, respectively.

He is a Professor with Grenoble University (Université Joseph Fourier), Grenoble, France, within the Grenoble Electrical Engineering Laboratory (G2ELab), in the field of power electronics. He is currently a Director of the G2ELab, after several years of leading the power electronics team. His first research interest concerned resonant converters.

Afterward, he promoted electromagnetic compatibility activities in the field of power electronics and developed a leading activity in the technological design of power converters.



Jean-Luc Schanen (M'99–SM'04) was born in 1968. He received the Diploma in electrical engineering and the Ph.D. degree from Grenoble Institute of Technology, Grenoble, France, in 1990 and 1994, respectively.

He is currently a Professor with Grenoble Institute of Technology. He has been with the Grenoble Electrical Engineering Laboratory (G2ELab), St. Martin d'Hères, France, since 1994, working in the field of power electronics. His main activities concern the technological design of power converters. His

research team uses (or develops, if not available) all kinds of modeling tools in order to improve the performance of power-electronic converters, including electromagnetic compatibility and thermal aspects.

Prof. Schanen was Chairman of the Power Electronics Devices and Components Committee of the IEEE Industry Applications Society between 2006 and 2007. He is a senior member of the IEEE Power Electronics Society and IEEE Industry Applications Society.



Philippe Loizelet received the Dipl. Ing. degree from Grenoble Institute of Technology, Grenoble France, in 1995.

From 1988 to 2000, he was with the Research and Development Department in drive activity of Schneider Electric. Since 2001, he has been with Schneider Toshiba Inverter Europe, Pacy sur Eure, France, where he is currently an R&D Engineer in the field of power electronic for ac drives.